International Journal of Rock Mechanics & Mining Sciences 60 (2013) 160–170

Contents lists available at SciVerse ScienceDirect

International Journal of Rock Mechanics & Mining Sciences

journal homepage: www.elsevier.com/locate/ijrmms

# Borehole stability analysis accounting for anisotropies in drilling to weak bedding planes

Jincai Zhang [1]

*Shell Exploration and Production Company, USA*

ARTICLE INFO

*Article history:*
Received 24 April 2012
Received in revised form
7 September 2012
Accepted 22 December 2012
Available online 1 February 2013

*Keywords:*
Borehole stability
Bedding planes
Anisotropy
In-situ stress
Weak rock strength
Time-dependent rock strength
Wellbore shear failure
Slip failure

ABSTRACT

Borehole instabilities pose significant challenges to drilling and completion operations, particularly in regions with weak bedding planes and pre-existing fractures where formations have strong anisotropies. The bedding planes, rock anisotropy, and their impacts on horizontal stresses are considered in the proposed model to improve borehole stability modeling. This improved model enables to calculate borehole failures and minimum mud weight along borehole trajectories with various drilling orientations versus bedding directions. Laboratory test data of rock compressive strengths are analyzed, and a new correlation is developed to allow for predicting uniaxial compressive strengths in weak rocks from sonic velocities. Time-dependent rock compressive strength is also examined to analyze the wellbore failure evolution with time. The slip failure gradient in the weak planes is derived, which can be used to model wellbore sliding/shear failure in the planes of weakness. The mud weight applied to prevent borehole shear failures in both intact rocks and ones with weak bedding planes can be obtained from the proposed model.



## 1. Introduction

Borehole instability is a major cause of borehole failures and represents a serious challenge in the drilling industry. A lack of accurate wellbore stability analysis brings many problems, such as borehole washouts, breakout, collapse, stuck pipes and drill bits, and losses of boreholes. Wellbore instability also adds to drilling time, increased costs, and sometimes leads to abandoning the well before it reaches its objective. Estimates put the cost of these issues at approximately 10% of total drilling time on average [1]. The relationship of mud weight and wellbore failures (Fig. 1) demonstrates that when the mud pressure is less than the pore pressure, the wellbore has splintering failure or washout. When the mud pressure is less than the shear failure gradient, the borehole has shear failure or breakout/collapse. If the mud weight is higher than the fracture gradient, the drilling-induced hydraulic fractures are generated, causing drilling mud losses or lost circulation. To maintain borehole stability, the applied mud weight should be in an appropriate range. The borehole failures can primarily be classified to the following four categories as illustrated in Fig. 1: (1) wellbore washouts or fluid kicks due to underbalanced drilling, where the mud weight is much less than the pore pressure; (2) wellbore breakouts or shear failures due to a low mud weight; (3) mud losses or lost circulation due to tensile failure (hydraulic fractures) induced by a high mud weight; and (4) rock failures or sliding related to pre-existing fractures.

Different analytical methods and numerical models have been used for borehole stability analyses [2–20]. However, borehole instability is still a main cause of borehole losses in difficult formations and conditions, such as unconsolidated formations, faulted and fractured rocks, weak planes, rubble zones, and salt structures. Therefore, more sophisticated geomechanical modeling is required for accessing the reservoirs under these difficult conditions. For instance, drilling along bedding planes and in depleted reservoirs is very risky [21]. When a well is drilled at shallow angles to thinly bedded shales, it is often highly unstable. Rock failure can occur as a result of rock strength anisotropy caused by weak bedding planes. In these cases, an increased mud weight while drilling is required. However, when the reservoir immediately beneath the bedded shales is depleted, the increased mud weight can lead to lost circulation. Modeling of this geomechanical environment presents many challenges and requires coupling the in-situ stress, pore pressure, mud pressure, and anisotropic effects of rock strengths and stresses. Borehole stability modeling with considerations of pre-existing fractures and planes of weakness in oil and gas wells has been reported (e.g., [17,21–28]), but failure mechanism of boreholes in planes of weakness is still not fully understood. This paper first introduces borehole stability analysis in isotropic rocks with emphasis on how to determine the input parameters for the modeling,

*E-mail address:* zhangjincai@yahoo.com
[1] Now with Hess Corporation.

1365-1609/$ - see front matter © 2012 Elsevier Ltd. All rights reserved.
http://dx.doi.org/10.1016/j.ijrmms.2012.12.025

including in-situ stress and rock strength. Then, the rock strength anisotropy and weak bedding plane impact on borehole stability are studied.

## 2. Borehole stability modeling in isotropic rocks

Borehole stability modeling for drilling operations is primarily to create a safe mud weight (mud pressure) window such that the designed mud density will be high enough to ensure borehole stability and low enough to not fracture the formation (i.e., mud losses do not occur), as shown in Fig. 1. Therefore, the safe mud weight should be greater than the pore pressure gradient and shear failure gradient and less than the fracture gradient. To determine the safe mud weight, the first step is to analyze the near wellbore stresses induced by drilling. Then using an appropriate failure criterion determines if the wellbore fails by comparing the wellbore stress to the rock strength. It is commonly assumed that in-situ stress consists of three mutually orthogonal principal stresses: vertical (overburden) stress ($\sigma_V$), minimum and maximum horizontal stresses ($\sigma_H$, $\sigma_h$). It is also assumed that the subsurface rocks are in the in-situ stress state prior to drilling. When a borehole is excavated, the stress redistribution near wellbore occurs causing stress changes around the wellbore compared to the in-situ or far-field stress. Fig. 2 shows the in-situ stress and near wellbore stresses induced by drilling. Borehole stability analysis is more complicated in an inclined borehole, because the far-field stress in the inclined borehole coordinate is no longer in the principal stress state, due to the shear stresses are introduced at the wellbore cross-section in the deviated borehole. Therefore, the principal in-situ stresses in the borehole local coordinate first need to be calculated for the inclined borehole, as shown in Fig. 2. Then, the wellbore stresses induced by drilling can be obtained if the in-situ stress and pore pressure are known, (see Appendix).

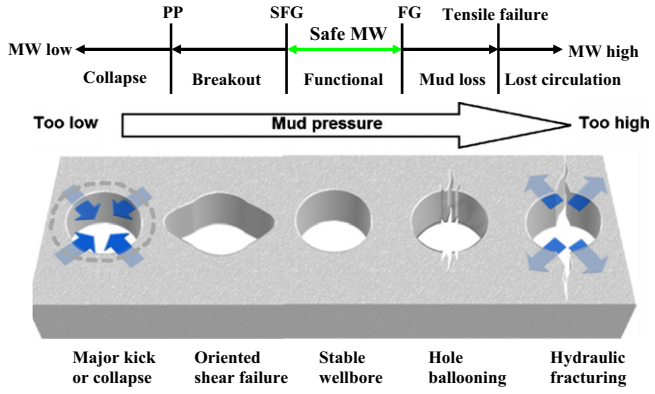


**Fig. 1.** Schematic relationship of mud pressure (mud weight, MW) and borehole failures.

To model the borehole stability, the following data are used as the primary inputs: (1) the in-situ stress and orientations; (2) pore pressure; (3) borehole trajectory; and (4) rock property and rock strength. Conventionally, the in-situ stress and rock strength can be obtained from the methods provided in literature (e.g., [29–31]). Pore pressures in most petroleum basins are not hydrostatic but overpressured. Special methods are needed to estimate the overpressures, which can be found in [32]. The following sections present some of these parameters and the conventional analytical modeling of wellbore stability.

### 2.1. The minimum horizontal stress in isotropic formations

The minimum stress is an important parameter because the fracture gradient can be calculated from the minimum stress. Normally, the minimum stress is the lower bound of the fracture gradient [16,32]. The minimum horizontal stress can be determined by direct measurements, i.e., via the universally accepted method of micro-hydraulic fracturing (e.g., [33]), or its oil field equivalent, the leak-off test (LOT) and extended leak-off test (XLOT) [34].

Using the uniaxial strain model, the minimum stress can be calculated if the overburden stress, pore pressure and Poisson's ratio are known [35]. In a normal faulting stress regime, the minimum horizontal stress is the minimum principal in-situ stress and can be obtained from the following equation:

$$\sigma_h = \frac{v}{1-v}\left(\sigma_V - \alpha p_p\right) + \alpha p_p \quad (1)$$

where $\sigma_h$ is the minimum horizontal stress; $\sigma_V$ is the overburden stress and can be obtained by integration of the bulk density of the formations; $p_p$ is the pore pressure; $\alpha$ is the Biot's constant; and $v$ is the Poisson's ratio.

The minimum horizontal stress decreases with reservoir depletion and can be obtained by substituting the reservoir pressure after depletion, $p_{pd}$, into Eq. (1) to replace $p_p$.

### 2.2. Determination of the maximum horizontal stress

When measured data (such as XLOT) are available, the maximum horizontal stress can be calculated from the fracture

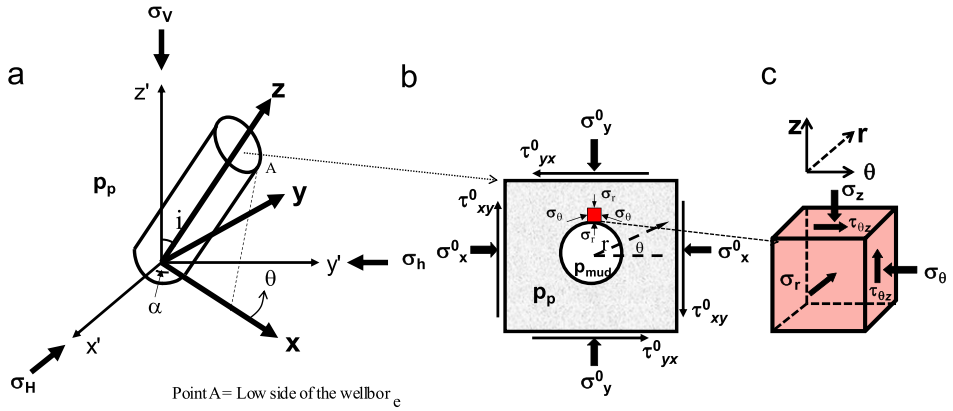


**Fig. 2.** Coordinates transformation between in-situ stress ($\sigma_V$, $\sigma_H$, $\sigma_h$) and local in-situ stress in an inclined borehole ($\sigma_x^0$, $\sigma_y^0$, $\sigma_z^0$, $\tau_{xy}^0$, $\tau_{yz}^0$, $\tau_{xz}^0$). (a). 3D view of an inclined borehole; (b). Local in-situ stresses and wellbore stresses in a cross-section perpendicular to the axial direction of the inclined borehole; (c). A cubic element showing normal and shear stresses at the wellbore wall.

breakdown pressure [34]. Li and Purdy [36] proposed an improved method compared to Zoback's model [30] to determine the maximum horizontal stress using observations of vertical borehole breakout angle if the rock uniaxial compressive strength is known, that is:

$$\sigma_H \le \frac{UCS+(q+1)p_{\mathrm{mud}}-\alpha(q-1)p_p-(1-2\cos 2\beta_b)\sigma_h+\sigma^{\Delta t}}{1+2\cos 2\beta_b} \quad (2)$$

where $UCS$ is the uniaxial compressive strength of the rock; $2\beta_b$ is the wellbore breakout angle; $p_{\mathrm{mud}}$ is the mud pressure; $q$ is a parameter related to rock internal friction angle, and $q=(1+\sin\phi)/(1-\sin\phi)$ or $q=[(\mu^2+1)^{1/2}+\mu)]^2$; $\phi$ is the angle of internal friction; $\mu$ is the friction coefficient of the rock; and $\sigma^{\Delta t}$ is the thermal stress. In some cases the temperature effect is small and can be neglected.

### 2.3. Compressive strength of rocks from sonic logs

Rock strength is a key input in borehole stability modeling. Rock strengths are preferably obtained from laboratory core tests and secondarily from correlations of the compressional velocity of sound. To estimate rock strength in all depth sections, the rock strength and sonic compressional velocity correlations can be used; however, they need to be calibrated to the rock strength from the lab core test data. The commonly used rock strength and sonic compressional velocity or transit time correlations are shown as follows.

Lal [37] presented the following correlation for shales in the Gulf of Mexico:

$$UCS=10(304.8/\Delta t-1) \quad (3)$$

where $UCS$ is in MPa; and $\Delta t$ is the transit time in μs/ft. Horsrud [38] proposed another correlation using a different method to fit the experimental data from the Tertiary shale specimens in the North Sea:

$$UCS=0.77(304.8/\Delta t)^{2.93} \quad (4)$$

These correlations are applicable in some Tertiary shales in the Gulf of Mexico and the North Sea.

Some high porosity (~20%) sandstones are weaker than shales, such as in the Tertiary formations in the Gulf of Mexico. In this case, the wellbore breakout or washout is expected while drilling and before the hole is cased. For weak sandstones of Tertiary formations in the Gulf of Mexico and North Sea, we obtain the following empirical equation to estimate $UCS$ based on the data presented in [16]:

$$UCS=0.68(304.8/\Delta t)^{2.5} \quad (5)$$

where $UCS$ is in MPa and $\Delta t$ is in μs/ft.

Fig. 3 demonstrates the rock uniaxial compressive strengths from core tests in sandstones, shales, and mixed lithology of shales and sandstones in the Gulf of Mexico [16]. The data have the following characteristics: (1) there are two groups in the rock strength data—a lower $UCS$ group and a higher $UCS$ group. Most rocks in the higher $UCS$ group are shale formations; (2) Lal's and Horsrud's correlations underestimate the strengths of shales, but overestimate the strength of high-porosity sandstones [16]. (3) $UCS$ in sandstones (circles in Fig. 3) is lower than that in shales; therefore, most sandstones are weak rocks, because of high porosity. Using Eq. (5), the $UCS$ in weak sandstones are calculated and compared to the core test data, as shown in Fig. 3. The figure shows that the calculated $UCS$ from Eq. (5) gives a reasonable prediction of rock strength in sandstones and mixed lithology. This weak rock strength correlation (Eq. (5)) may also be suitable for weak shales, as shown in Fig. 3.

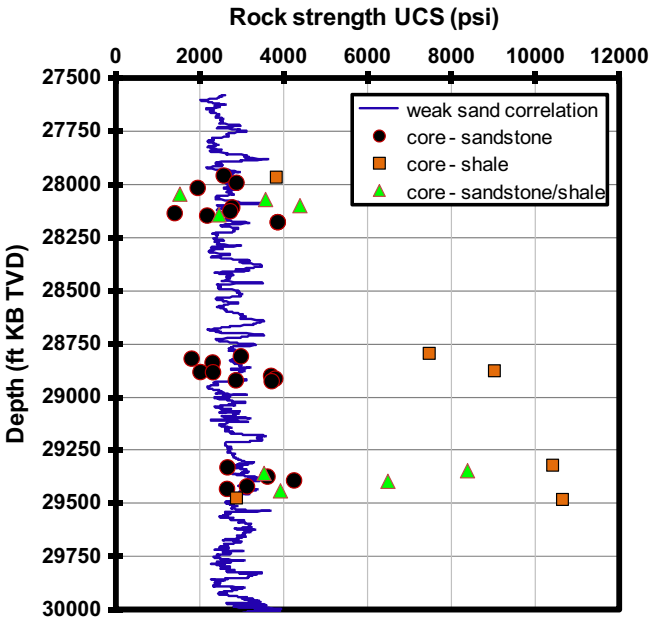


**Fig. 3.** Rock uniaxial compressive strength ($UCS$, 1 MPa ≈ 145 psi) obtained from lab compressive tests (Data points: circles for sandstones, squares for shales and triangles for mixed lithology) and calculated from sonic transit time ($\Delta t$) by using the weak rock correlation (Eq. (5)).

For stronger sandstones (porosity < 10%), there are a number of correlations to calculate rock strengths (e.g., [29–30]).

### 2.4. Time-dependent compressive strength

Laboratory experiments have demonstrated that rock compressive strength decreases as time increases [39–41]. This is mainly caused by rock relaxation or creep, i.e., rock strain increases with time even under a constant loading stress. Therefore, when subjected to a constant stress even smaller than the rock strength, rock deforms and eventually fails after a time delay because of creep. The same phenomenon is observed in drilling, i.e., hole deterioration with time. For example, wellbore breakouts increase greatly from the caliper logs performed a number of hours later compared to the caliper log run earlier in the same depth interval [42], as shown in Fig. 4. This is partially because the rock compressive strength decreases as the borehole exposure time increases. This is why it needs to reduce exposure days of an open hole and case it soon after drilling to avoid wellbore instability. Based on the experimental results [39–41,43], we propose the following empirical equation to describe the rock strength reduction with time:

$$UCS=UCS_0(1-C\log t) \quad (6)$$

where $UCS_0$ is the original $UCS$ without time effect; $t$ is the rock exposure time in seconds ($t \ge 1$); $C$ is a constant and can be obtained from lab experiments; $C=0.24$ for granite [41] and it is smaller for sedimentary rocks, and can be obtained by calibrating borehole breakouts to borehole exposure time.

### 2.5. Wellbore shear failure gradient and fracture gradient

For borehole stability analysis, we need to determine (1) the minimum mud weight (shear failure gradient) to maintain the wellbore from shear failure (wellbore collapse); (2) the maximum mud weight to not cause wellbore tensile failure (unintentionally hydraulic fracturing). Practically, the fracture gradient is the maximum mud weight in a particular drilling section in terms

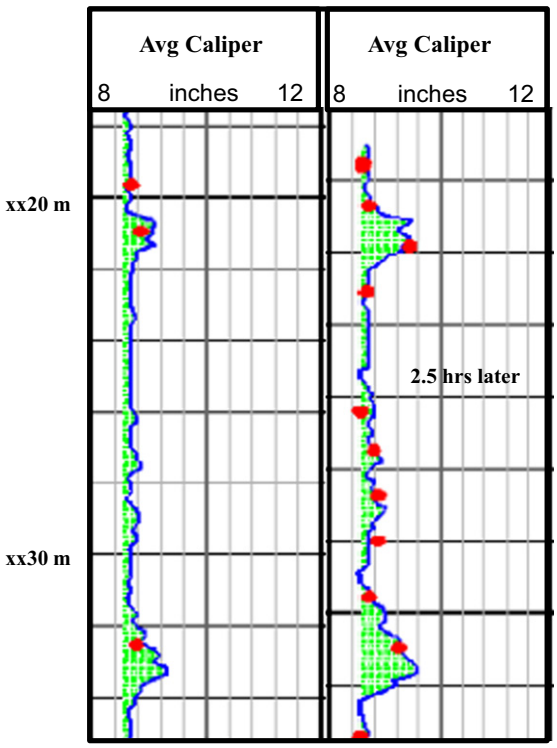


**Fig. 4.** Caliper logs in the same depth intervals observed between two logging runs with 2.5 h of elapsed time. It shows that the hole diameters/breakouts (shaded parts) increase with time (modified from [42]).

of avoiding hydraulic fracturing and mud losses. The lower bound of fracture gradient can be calculated from Eq. (1), and the most likely fracture gradient (pressure) can be obtained from [32] as following:

$$P_{FP} = \frac{3v}{2(1-v)}\left(\sigma_V - \alpha p_p\right) + \alpha p_p \tag{7}$$

where $P_{FP}$ is the most likely fracture pressure.

The minimum mud pressure required to keep the borehole stability may also be named to be the collapse pressure or shear failure pressure. It can be expressed in the gradient form (i.e., the shear failure pressure divided by the true vertical depth) as the shear failure gradient or the minimum mud weight. The shear failure pressure can be analytically calculated from Kirsch's elastic solution (e.g., [29,31]).

The effective stress at the wellbore wall in a vertical or horizontal well can be obtained from Eq. (A3) of the Appendix and written as follows:

$$\begin{aligned}\sigma'_r &= p_{\mathrm{mud}} - \alpha p_p \\ \sigma'_\theta &= \sigma_{\max} + \sigma_{\min} - \alpha p_p - p_{\mathrm{mud}} - 2(\sigma_{\max} - \sigma_{\min})\cos 2\theta \\ \sigma'_z &= \sigma_{\mathrm{axis}} - \alpha p_p - 2v(\sigma_{\max} - \sigma_{\min})\cos 2\theta\end{aligned} \tag{8}$$

where $\sigma'_r$, $\sigma'_\theta$, and $\sigma'_z$ are the effective radial, tangential, and axial stresses at the wellbore wall, respectively; $v$ is the Poisson's ratio; $\sigma_{\max}$, $\sigma_{\min}$ are the in-situ maximum and minimum principal stresses in the wellbore cross-section, respectively. For a vertical well, $\sigma_{\max}=\sigma_H$, $\sigma_{\min}=\sigma_h$ and $\sigma_{\mathrm{axis}}=\sigma_V$; for a horizontal well drilled in the minimum stress direction in normal faulting stress regime, $\sigma_{\max}=\sigma_V$, $\sigma_{\min}=\sigma_H$ and $\sigma_{\mathrm{axis}}=\sigma_h$; $\sigma_V$, $\sigma_H$, and $\sigma_h$ are the vertical stress, maximum and minimum horizontal stresses, respectively; $\theta=0^\circ$ represents the direction of the maximum in-situ stress ($\sigma_{\max}$) in the cross section of the borehole (Fig. 2b); and $\theta=90^\circ$ represents the direction of the minimum in-situ stress ($\sigma_{\min}$).

This equation is valid for isotropic rocks and can also be used in the isotropic planes for the transversely isotropic rocks. The three effective stresses ($\sigma'_r$, $\sigma'_\theta$, $\sigma'_z$) in the above equations are the principal stresses. Therefore, the Mohr–Coulomb failure criterion can be applied for shear failure analysis with the assumption that the effective tangential and radial stresses are the principal maximum and minimum stresses. The Mohr–Coulomb failure criterion assumes that the effective principal stresses satisfy the following relationship before the shear failure takes place:

$$\sigma'_1 \le UCS + q\sigma'_3 \tag{9}$$

where $\sigma'_1$, $\sigma'_3$ are the maximum and minimum effective principal stresses at the wellbore wall.

Substituting Eq. (8) to Eq. (9), noticing $\sigma'_1=\sigma'_\theta$ and $\sigma'_3=\sigma'_r$, the mud pressure, or shear failure pressure $p_m$, to prevent shear failure around the wellbore wall can be obtained as the following equation:

$$p_m = \frac{\sigma_{\max} + \sigma_{\min} - 2(\sigma_{\max} - \sigma_{\min})\cos 2\theta - UCS + \alpha(q-1)p_p}{q+1} \tag{10}$$

where $UCS$ can be calculated by $UCS=(2c\cos\phi)/(1-\sin\phi)$; $q=(1+\sin\phi)/(1-\sin\phi)$; $p_m$ is the shear failure pressure; $\phi$ is the angle of internal friction; $c$ is the cohesion of the rock; and $p_p$, $\sigma_{\max}$, $\sigma_{\min}$ are as defined before.

When $\theta=90^\circ$ (the minimum in-situ stress direction), the wellbore wall has the maximum effective tangential stress (from Eq. (8)). Therefore, the minimum mud pressure to maintain the entire wellbore wall without any shear failures ($p_{\min}$) can be calculated from Eq. (10) with $\theta=90^\circ$ as following:

$$p_{\min} = \frac{3\sigma_{\max} - \sigma_{\min} - UCS + \alpha(q-1)p_p}{q+1} \tag{11}$$

Eqs. (10) and (11) illustrate that the minimum mud weight is heavily dependent on the pore pressure and rock strength. Therefore, accurate prediction of the pore pressure is of vital importance for determining the optimal mud weight for drilling operations. Other failure criteria may also be applied for shear failure analysis, such as Modified Lade, Drucker–Prager, Mogi [2,8,11,31,44].

### 2.6. Comparison with field data

A deepwater oil field with water depth of 3560 ft in the Gulf of Mexico [16] is examined for post-well borehole stability. The studied borehole is a vertical well, and the rocks in studied sections are weak shales and high-porosity sandstones with low *UCS*; therefore, wellbore breakouts took place in several sections. Using Mohr–Coulomb failure criterion, the shear failure gradient is calculated by Eq. (11) based on the weak rock strength and sonic transit time correlation (Eq. (5)). The calculated shear failure gradient is compared to the downhole mud density or the equivalent circulating density (ECD) while drilling, as shown in Fig. 5. The figure shows that the ECD should be 13–14 ppg to avoid borehole breakouts from 28,000 to 28,360 ft, and a slightly higher ECD (0.2 ppg more) than the applied one is needed to keep wellbore on-gauge from 28,650 to 29,220 ft. It should be noted that in the central interval between 28,900 ft and 28,970 ft, the sonic data are not so reliable, causing the rock strength (calculated from sonic data) and the calculated shear failure gradient to be unreliable. In addition, the pore pressure uncertainty in the section of 28,000–28,360 ft (no measured pore pressure data available) may also cause the uncertainty in shear failure gradient calculation.

The weak rock strength correlation (Eq. (5)) is used to calculate *UCS* which is calibrated from the lab test data. The calculated *UCS* values are also compared to the ones obtained from Lal's correlation, as shown in Fig. 5. It shows that the strength difference can reach about 1000 psi. Fig. 5 illustrates that the wellbore breakout

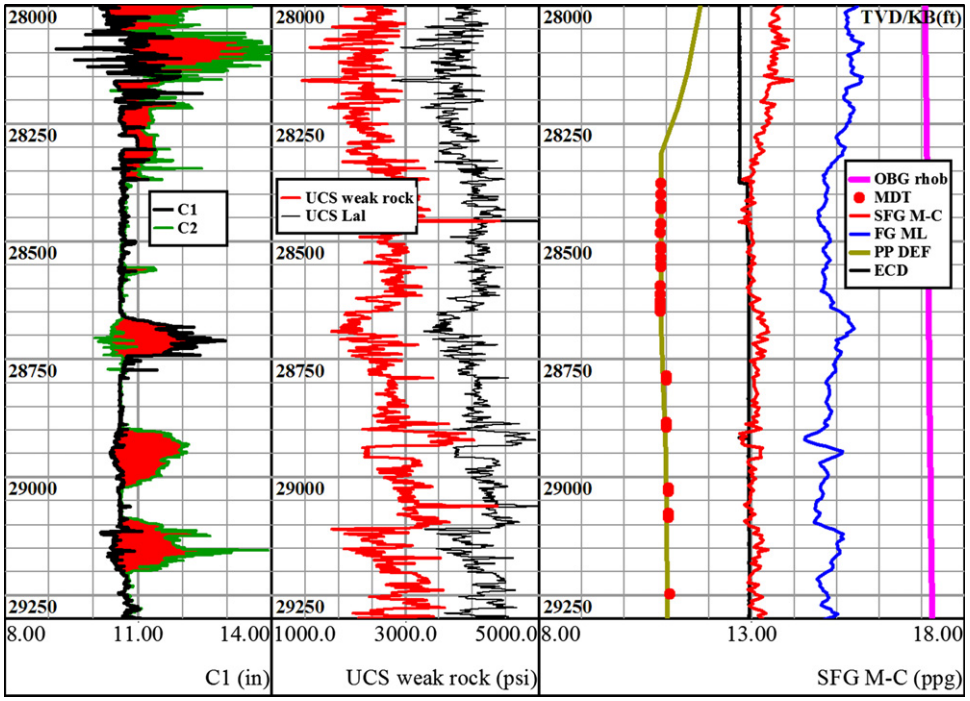


**Fig. 5.** Post-well borehole stability analysis. The left track shows the 4-arm caliper log where the shaded parts are wellbore breakouts. The middle track presents *UCS* values calculated from sonic transit time using the proposed method (Eq. (5)) and Eq. (3) after Lal's correlation. The right track shows pore pressures (PP DEF) with measured formation pressure from MDT method, calculated shear failure gradient (SFG M-C) from Eq. (11), the ECD, fracture gradient (FG ML, calculated from Eq. (7)), and overburden stress gradient (OBG rhob).

happens mainly in the sections where the *UCS* values are low ($<3000$ psi). Besides low ECD, the low *UCS* or maybe the weak bedding planes is the main reason to cause wellbore breakout.

## 3. Borehole stability analysis with weak/bedding plane effects

### 3.1. Wellbore failures in the rocks with pre-existing fractures and bedding planes

Wellbore shear failure owing to low mud weight normally forms a symmetrical breakout along the local in-situ minimum stress direction (Fig. 6). However, in the formation with pre-existing fractures and planes of weakness, wellbore failures are different from the typical mode. When borehole is intersected by a weak rock zone, the failures occur not only along the in-situ minimum stress direction, but also near and in the weak rock area. This is because the weak rock has a much lower strength and, furthermore, there is a much larger stress concentration triggered at the interface between the strong rock and weak planes [45].

Fig. 7 presents a laboratory modeling of wellbore failure caused by bedding planes. It shows that a layered model, expertly fabricated by Bandis in 1987 [47], consists of thinly-bedded sandstones and micaceous inter-layers. The steeply inclined beddings allow a buckling mode of deformation to develop, causing an elliptical failure zone. Such buckling mechanisms are common in thinly-bedded rocks and presumably can compromise the integrity of horizontal wells [47]. Laboratory tests in shales with slightly inclined dipping show that the wellbore failures are also highly related to the planes of weakness [23].

### 3.2. Horizontal stresses in transversely isotropic rocks

The rock anisotropy also causes the anisotropy in the in-situ stress. For instance, in the transversely isotropic formations (i.e., the formations with the symmetric axis in the vertical direction), the horizontal minimum stress in the normal faulting stress regime can be written in the following forms [49]:

Under uniaxial strain condition:

$$\sigma_h = \alpha p_p + \frac{E\nu'}{E'(1-\nu)}\left[\sigma_V - \alpha(1-\xi)p_p\right] \tag{12a}$$

Under uniform horizontal strains:

$$\sigma_h = \alpha p_p + \frac{E\nu'}{E'(1-\nu)}\left[\sigma_V - \alpha(1-\xi)p_p\right] + \frac{E}{1-\nu^2}\varepsilon_h + \frac{E\nu}{1-\nu^2}\varepsilon_H \tag{12b}$$

where $E$ is the Young's modulus in the plane of isotropy; $E'$ is the Young's modulus normal to the plane of isotropy; $\nu$ is the Poisson's ratio in the plane of isotropy; $\nu'$ is the Poisson's ratio for stress acting normal to the plane of isotropy; $\xi$ is the poroelastic constant; and $\varepsilon_H$ and $\varepsilon_h$ are the tectonic strains in the maximum and minimum horizontal stress directions, respectively.

### 3.3. Borehole stability analysis with consideration of weak bedding planes

In general, rocks or rock masses are more or less anisotropic, particularly, for example, the jointed rock masses or slates, shales, and schists. Experimental study of the stress states on failure behavior in anisotropic rocks using the triaxial and poly-axial compression tests ($\sigma_1 > \sigma_2 \geq \sigma_3$) demonstrate that the strengths of the anisotropic rocks vary significantly with the directions of the applied stress and bedding planes (e.g., [50–57]). Fig. 8 shows schematically the experimental method and the observed compressive strength variations in the rock specimen with effects of the weak planes. Fig. 8(b) presents schematically the peak principal stress ($\sigma_1$) at rock failures as a function of angle $\beta$. Failure of the anisotropic rocks is most likely to occur when the

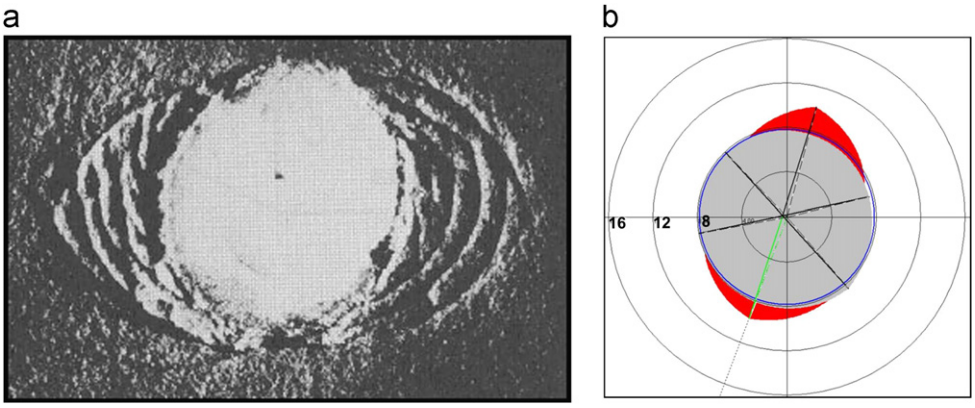


**Fig. 6.** Wellbore breakouts in homogeneous rocks (a) from laboratory test [46]; (b) processed from downhole 6-arm caliper log (the shaded area is the breakout and the unit is in inches).

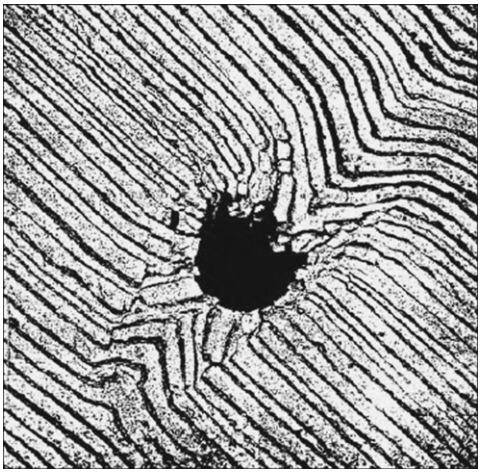

**Fig. 7.** Wellbore failure when penetrating steeply dipping thinly-cycled beds [48].

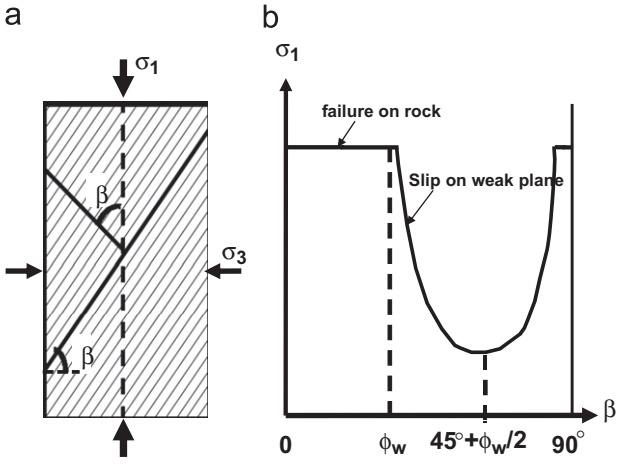


**Fig. 8.** (a). Transversely isotropic specimen with bedding/weak planes in a triaxial compressive test; (b). Schematic rock peak strength variation with the angle, $\beta$, in the triaxial test at a constant confining stress ($\sigma_3$ ) inspired by experimental tests and Eq. (13) [58].

angle, $\beta$, is nearly equal to the shear failure angle ($\eta$) of isotropic rocks (Fig. 9), i.e., when $\beta=45^\circ+\phi/2$.

Using Mohr–Coulomb failure criterion, Jaeger et al. [58] gave an equation to calculate the maximum and minimum principal stresses associated with the weak plane sliding along pre-existing planes of weakness for a rock mass having a set of parallel planes of weakness. This equation can be expressed in the following form in terms of effective stresses:

$$\sigma'_1-\sigma'_3=\frac{2(c_w+\mu_w\sigma'_3)}{(1-\mu_w\cot\beta)\sin 2\beta} \tag{13}$$

where $\beta$ is the angle between the directions of $\sigma'_1$ and the normal of the planes of weakness, and $\phi_w<\beta<90^\circ$; $\sigma'_1$, $\sigma'_3$ are the maximum and minimum principal effective stresses, respectively; $c_w$ is the cohesion of the planes of weakness; $\mu_w$ is the coefficient of internal friction in the planes of weakness; and $\mu_w=\tan\phi_w$; $\phi_w$ is the angle of internal friction in the planes of weakness.

The value of $\sigma_1$ required to cause failure, as given by Eq. (13), trends to infinity as $\beta\to 90^\circ$ or $\beta\to\phi_w$ (i.e., failure in the rock). In other words, when $0<\beta<\beta$ and $\beta=90^\circ$, the planes of weakness have no impact on the rock strength. For angles in between those two values, failure will occur at a finite value of $\sigma_1$ that varies with $\beta$ (i.e., failure in the weak planes), as shown in Fig. 8b. The minimum strength occurs when (refer to Fig. 8b):

$$\beta_{\min}=45^\circ+\varphi_w/2 \tag{14}$$

According to Biot's law of effective stress, the principal effective stresses ($\sigma'_1$ and $\sigma'_3$) at wellbore wall in each borehole section (e.g., Fig. 10) can be derived from the stress tensor at the wellbore wall. For instance, we can obtain the principal effective stresses at wellbore wall in a vertical or horizontal well from Eq. (8). Then, by substituting the principal effective stresses ($\sigma'_1$ and $\sigma'_3$, or $\sigma'_\theta$ and $\sigma'_r$ in Eq. (8)) into Eq. (13) we can obtain the minimum mud weight ($p_w$) for preventing wellbore sliding in the weak planes. For the shear failure with consideration of a set of parallel planes of weakness in a horizontal or vertical wellbore, the following equation can be obtained to calculate the minimum mud pressure ($p_w$) for preventing wellbore sliding (shear failure) in the weak planes. This minimum mud pressure ($p_w$) is denoted to be the weak plane "slip failure pressure," and its gradient is called "slip failure gradient":

$$p_w=\frac{[\sigma_{\max}+\sigma_{\min}-2(\sigma_{\max}-\sigma_{\min})\cos 2\theta](1-\mu_w\cot\beta)\sin 2\beta-2c_w+2\mu_w p_p}{2[\mu_w+(1-\mu_w\cot\beta)\sin 2\beta]} \tag{15}$$

where $p_w$ is the required mud weight to prevent wellbore slip in the weak planes or slip shear failure pressure; $\theta$ is the angle defined in Fig. 10; $\beta$, $\mu_w$ and $c_w$ are defined as before; $\sigma_{\max}$, $\sigma_{\min}$ are the maximum and minimum in-situ principal stresses, respectively. For example, for a horizontal well drilled in the minimum stress direction in normal faulting stress regime, $\sigma_{\max}=\sigma_V$ and $\sigma_{\min}=\sigma_H$. For a vertical well, $\sigma_{\max}=\sigma_H$ and $\sigma_{\min}=\sigma_h$.

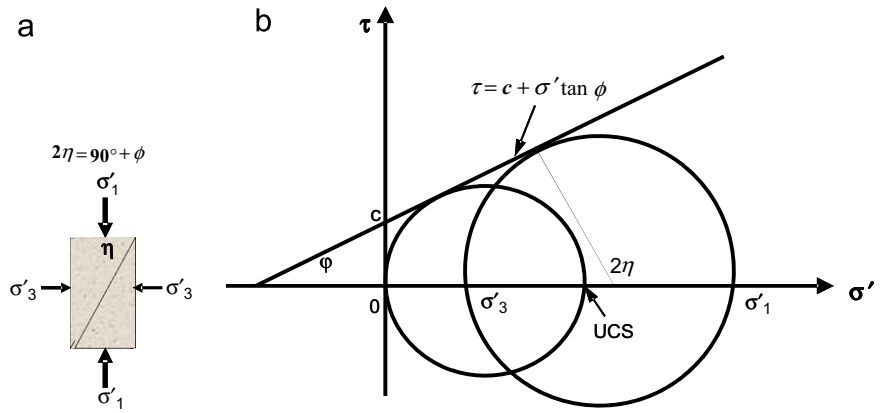


**Fig. 9.** Shear failure plane (a) and Mohr circle (b) in an isotropic rock specimen. $c$ is the cohesion of the rock; $\phi$ is the angle of internal friction of the rock; and $\eta$ is the angle of shear failure plane.

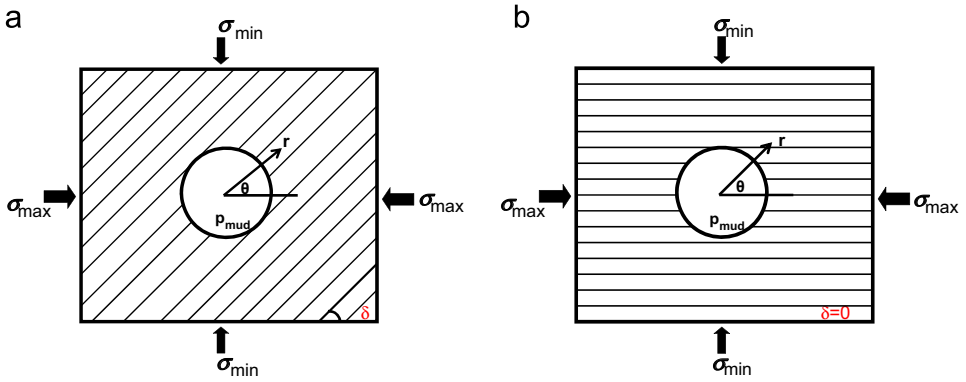


**Fig. 10.** The cross sections (perpendicular to borehole axis direction) of two boreholes drilled in rocks with different orientations of the bedding planes (schematic representations in two cases) in anisotropic in-situ stress field.

It should be noted that the angle, $\beta$, varies around the wellbore cross-section and with borehole trajectory, even the dip and strike of the weak planes kept unchanged. This means that $\beta$ is a function of $\theta$. When the angle, $\beta$, meets Eq. (14), it has the highest slip failure pressure because the bedding planes have the lowest strength. Eq. (15) is only applicable for vertical and horizontal boreholes. For inclined boreholes, the semi-analytical solution is obtained, as presented in the Appendix.

### 3.4. *Illustrative examples for borehole stability with consideration of weak bedding planes*

We examine the borehole stability with impact of the weak bedding planes in a horizontal deepwater well (water depth of about 5000 ft) drilled in the minimum horizontal stress direction. The following parameters at the studied depth of 12,800 ft TVD are obtained from post-drill analysis: the maximum stress gradient of $\sigma_{max}=\sigma_V=13.8$ ppg, the minimum stress gradient at the borehole cross-section of $\sigma_{min}=\sigma_H=13$ ppg, and pore pressure gradient of $p_p=10.8$ ppg. The rock strength parameters are as follows: uniaxial compressive strength, $UCS=2995.2$ psi; internal friction angle, $\phi=30^\circ$.

A set of weak planes, as shown in Fig. 10(a), has an angle of $\delta=35^\circ$ to the maximum stress ($\sigma_{max}$ or $\sigma_V$) direction at the wellbore section. The weak planes have the following strength parameters: cohesion, $c_w=199.7$ psi; internal friction angle, $\phi_w=14.5^\circ$.

It should be mentioned that $\beta$ is a function of $\sigma_1$ and angles of $\delta$ and $\theta$, as defined in Figs. 8 and 10. In this case, $\beta=|\theta-\delta|$. Using Eq. (15), the slip failure pressure around the wellbore wall can be calculated. We only present the results in a half circumference of the wellbore wall (i.e., $\theta$ from 0 to 180°) because of symmetry, as shown in Fig. 11.

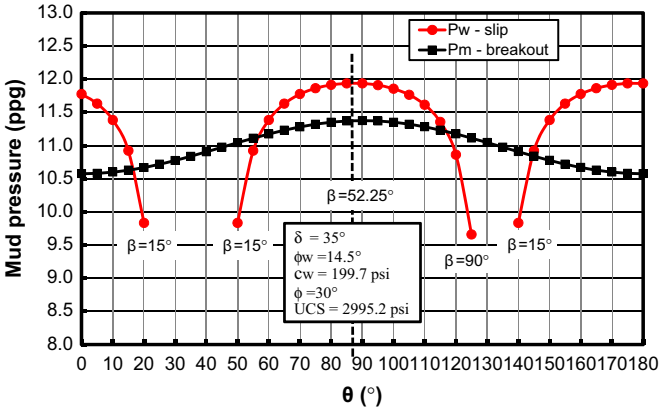


**Fig. 11.** The slip failure gradient ("$p_w$—slip" in the figure) caused by weak planes and the shear failure gradient ("$p_m$—breakout" in the figure) without the weak plane effects along the half circumference of the wellbore wall calculated from Eqs. (10) and (15). The angle between the bedding orientation and the maximum in-situ stress direction ($\sigma_{max}$) is $\delta=35^\circ$, as shown in Fig.10(a).

Fig. 11 displays the calculated slip failure gradient caused by weak bedding planes (presented as "$p_w$–slip" in Fig. 11) from Eq. (15) and shear failure gradient (without bedding plane effect, "$p_m$–breakout" in Fig. 11) from Eq. (10). As expected that the maximum shear failure gradient appears in the minimum in-situ stress direction ($\theta=90^\circ$, refer to Fig. 10(a) and 11), which is the

reason why the borehole breakout always occurs in the minimum stress direction for a horizontal or vertical well without impact of weak planes/fractures. However, with impact of weak planes, the slip failure gradient has a very different behavior. The maximum slip failure gradient, "$p_w$–slip" in Fig. 11, occurs when the bedding plane has a minimum strength, i.e., the angle $\beta$ meets Eq. (14). Therefore, the location where maximum slip failure gradient occurs depends upon $\phi_w$ and $\delta$. Thus, the slip failure locations and directions do not follow the conventional borehole breakout direction. Fig. 11 also indicates that the slip failure gradient varies markedly around wellbore in different locations owing to the fact that the peak strength of the weak planes varies significantly with the angle $\beta$, as shown in Fig. 8(b). When the strong rock layers are carrying most of the load (e.g., $\beta < \phi_w$), the wellbore failure will primarily take place in the strong rock layers. In other words, the slip failure in the weak planes only takes place when $\phi_w < \beta < 90^\circ$. Fig. 11 shows these cases. For instance, when $\beta < 14.5^\circ = \phi_w$, the slip failure gradient is smaller than the shear failure gradient, "$p_m$–breakout"; in this case, the wellbore should first have shear failure in the rock. When $14.5^\circ < \beta < 90^\circ$, the slip failure gradient is greater than the shear failure gradient; therefore, the wellbore should first demonstrate slip failure in the weak planes. It should be mentioned that the symmetric plane of the slip failure is in the locations of $\theta = \delta$, and $\theta = 180^\circ + \delta$ ($\delta = 35^\circ$ in Fig. 11).

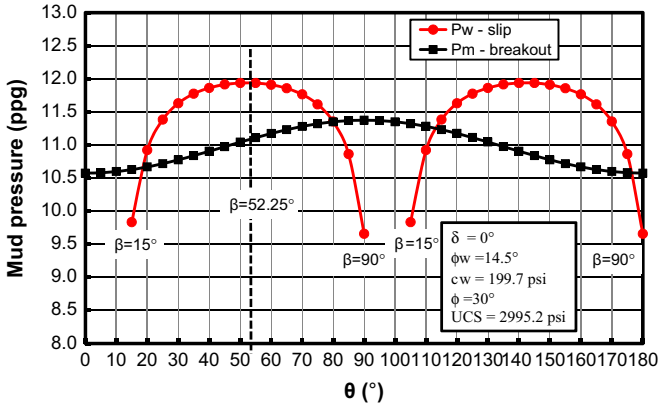


**Fig. 12.** Same as Fig. 11. The angle between the bedding orientation and the maximum in-situ stress direction ($\sigma_{max}$) $\delta = 0^\circ$, as shown in Fig. 10(b).

Fig. 12 shows another example for comparison of the slip failure gradient and shear failure gradient. In this case, only the angle of the weak planes changed, as shown in Fig. 10(b) with $\delta = 0^\circ$. It again indicates that the wellbore slip failure depends strongly on the orientation of weak planes, $\delta$, and the internal friction angle of the bedding planes, $\phi_w$.

Based on the above analyses, Fig. 13 gives an illustrative representation of wellbore slip failures caused by weak planes from the calculations in Figs. 11 and 12. If the applied mud weight (or ECD) is less than the calculated slip failure gradient, the slip failure will occur first in the weak planes. It should be noted that the maximum slip failure is not in the minimum stress direction like conventional breakout is. Instead, the maximum slip failures occur in two directions, and the maximum failure has an angle with the minimum or maximum in-situ stress direction, as shown in Fig. 13. The angle ($\psi$) depends upon the bedding orientation, $\delta$, and the internal friction angle of the bedding plane, $\phi_w$, as shown in the following:

$$\psi = \beta_{min} + \delta \tag{16}$$

or

$$\psi = 45^\circ + \delta + \varphi_w/2 \tag{17}$$

where $\psi$ is the angle between the maximum slip failure and the minimum or maximum in-situ stress direction, and the angle starts from the direction of $\sigma_{max}$ or $\sigma_{min}$ anticlockwise to the maximum slip failure area, as shown in Fig. 13.

However, if the applied mud weight (or ECD) while drilling is less than the slip failure gradient as well as the shear failure gradient (e.g., mud weight < 11.2 ppg in the case shown in Fig. 11), the slip failure in weak planes and shear failure in the rock will take place together and overlap, which will deteriorate wellbore stability and increase failure areas. Because the maximum shear failure takes place in the minimum stress direction and the slip failure also occurs near this location, this area will have the largest failure zone, as illustrated in Fig. 13(a). Fig. 13(b) illustrates that the shear and slip failures occur in the different locations and the wellbore failure area is very different from one in the intact rock (Fig. 6).

## 4. Conclusions

Borehole stability modeling is critically important for drilling, particularly in the down-dip direction of weak planes. In this

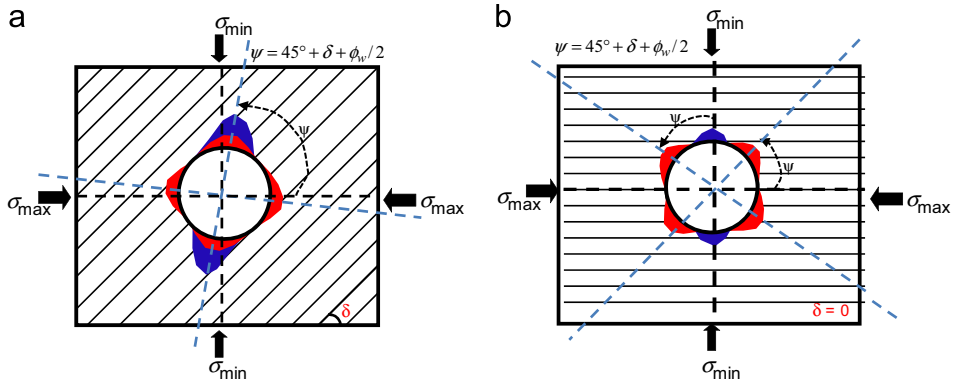


**Fig. 13.** Schematic presentations of wellbore shear failures and slip failures caused by the weak planes for two wellbores penetrating in weak bedding planes. The maximum slip failure direction is no longer in the minimum in-situ stress ($\sigma_{min}$) direction, but with an angle of ($\psi$) to the minimum or maximum in-situ stress direction. The red area represents the failures caused by the slip failure in the weak planes. The blue areas show the schematic failure zones caused by the shear failure in the rock. (a) a borehole cross-section that the angle between the bedding orientation and the maximum in-situ stress direction ($\sigma_{max}$) is $\delta = 35^\circ$. The failures are deteriorated because of overlapping of the slip failure in the weak planes and the shear failure in the rock. (b) a borehole cross-section that the angle between the bedding orientation and the maximum in-situ stress direction ($\sigma_{max}$) is $\delta = 0^\circ$. (For interpretation of the references to color in this figure legend, the reader is referred to the web version of this article.)

paper, laboratory test data of rock strengths in weak rocks were analyzed and a new correlation was developed to predict weak rock strength from sonic velocities. This can be used to predict high-porosity sandstones and weak shales in Tertiary formations.

Bedding planes and rock anisotropy were considered to improve borehole stability modeling. The improved borehole stability model enables to calculate wellbore failures along borehole trajectories with various drilling orientations versus bedding directions. Wellbore failure behaves differently with impact of weak bedding planes. The maximum slip failure occurs in which the bedding plane has a minimum strength. The slip failure locations and directions do not follow the conventional wellbore breakout direction but depend upon the internal friction angle and the orientation of the bedding planes. Furthermore, the wellbore slip failures occur in two directions and the failure directions have angles with the two local in-situ stress directions. Borehole stability analysis needs to consider both effects of shear failure in the rocks and slip failure in the weak planes. When the slip failure and shear failure overlap, the borehole instability deteriorates and failure areas increase.

## Acknowledgements

The author thanks the reviewers and editors for their constructive comments and suggestions in improving the manuscript.

## Appendix: Elastic Solution for Inclined Borehole Stability

For an inclined borehole the in-situ stress in a cross-section perpendicular to the wellbore axis can be expressed as following [59,31]:

$$\begin{aligned}
\sigma_x^0 &= \left(\sigma_H\cos^2\alpha+\sigma_h\sin^2\alpha\right)\cos^2 i+\sigma_V\sin^2 i\\
\sigma_y^0 &= \sigma_H\sin^2\alpha+\sigma_h\cos^2\alpha\\
\sigma_z^0 &= \left(\sigma_H\cos^2\alpha+\sigma_h\sin^2\alpha\right)\sin^2 i+\sigma_V\cos^2 i\\
\tau_{xy}^0 &= \frac{\sigma_h-\sigma_H}{2}\sin 2\alpha\,\cos i\\
\tau_{yz}^0 &= \frac{\sigma_h-\sigma_H}{2}\sin 2\alpha\,\sin i\\
\tau_{xz}^0 &= \frac{\sigma_H\cos^2\alpha+\sigma_h\sin^2\alpha-\sigma_V}{2}\sin 2i
\end{aligned} \tag{A1}$$

where $i$ is the borehole inclination, for a vertical well $i=0^\circ$ and for a horizontal well $i=90^\circ$; $\alpha$ is the angle of drilling direction with respect to $\sigma_H$ direction of the borehole, as shown in Fig. 2; $\sigma_x^0$, $\sigma_y^0$, $\sigma_z^0$, $\tau_{xy}^0$, $\tau_{yz}^0$, $\tau_{xz}^0$ are the in-situ stresses in an inclined borehole as shown in Fig. 2(b).

When an inclined borehole is drilled in the rock situated in the in-situ stress state (as shown in Eq. (A1)), the stress redistribution (near-field stresses) near wellbore wall occurs. This stress redistribution in the wellbore section (Fig. 2b) can be expressed in the following form using elastic plane strain model (e.g., [2]) in the polar system ($r$, $\theta$, $z$):

$$\begin{aligned}
\sigma_r &= \frac{\left(\sigma_x^0+\sigma_y^0\right)}{2}\left(1-\frac{R^2}{r^2}\right)+\frac{\left(\sigma_x^0-\sigma_y^0\right)}{2}\left(1-\frac{4R^2}{r^2}+\frac{3R^4}{r^4}\right)\cos 2\theta\\
&\quad+\tau_{xy}^0\left(1-\frac{4R^2}{r^2}+\frac{3R^4}{r^4}\right)\sin 2\theta+p_{\mathrm{mud}}\frac{R^2}{r^2}\\
\sigma_\theta &= \frac{\left(\sigma_x^0+\sigma_y^0\right)}{2}\left(1+\frac{R^2}{r^2}\right)-\frac{\left(\sigma_x^0-\sigma_y^0\right)}{2}\left(1+\frac{3R^4}{r^4}\right)\cos 2\theta\\
&\quad-\tau_{xy}^0\left(1+\frac{3R^4}{r^4}\right)\sin 2\theta-p_{\mathrm{mud}}\frac{R^2}{r^2}\\
\sigma_z &= \sigma_z^0-2\nu\left(\sigma_x^0-\sigma_y^0\right)\frac{R^2}{r^2}\cos 2\theta-4\nu\tau_{xy}^0\frac{R^2}{r^2}\sin 2\theta\\
\tau_{r\theta} &= \left(\frac{\sigma_x^0-\sigma_y^0}{2}\sin 2\theta+\tau_{xy}^0\cos 2\theta\right)\left(1+\frac{2R^2}{r^2}-\frac{3R^4}{r^4}\right)\\
\tau_{rz} &= \left(\tau_{yz}^0\sin\theta+\tau_{xz}^0\cos\theta\right)\left(1-\frac{R^2}{r^2}\right)\\
\tau_{\theta z} &= \left(-\tau_{xz}^0\sin\theta+\tau_{yz}^0\cos\theta\right)\left(1+\frac{R^2}{r^2}\right)
\end{aligned} \tag{A2}$$

where $\sigma_r$, $\sigma_\theta$, $\sigma_z$, $\tau_{r\theta}$, $\tau_{rz}$, $\tau_{\theta z}$ are the radial, tangential, axial normal stresses, and shear stresses near the wellbore wall in the wellbore cross-section (Fig. 2b), respectively; $p_{\mathrm{mud}}$ is the mud pressure; $\theta$ is the angle indicating the orientation of the stresses around the wellbore circumference and measured from the $x$-axis (Fig. 2a, b).

The normal stresses and shear stresses at the wellbore wall (when $r=R$, as shown in Fig. 2c) for an inclined borehole can be obtained from Eq. (A2) in the following:

$$\begin{aligned}
\sigma_r &= p_{\mathrm{mud}}\\
\sigma_\theta &= \sigma_x^0+\sigma_y^0-2\left(\sigma_x^0-\sigma_y^0\right)\cos 2\theta-4\tau_{xy}^0\sin 2\theta-p_{\mathrm{mud}}\\
\sigma_z &= \sigma_z^0-\nu[2\left(\sigma_x^0-\sigma_y^0\right)\cos 2\theta+4\tau_{xy}^0\sin 2\theta]\\
\tau_{\theta z} &= 2\left(-\tau_{xz}^0\sin\theta+\tau_{yz}^0\cos\theta\right)\\
\tau_{r\theta} &= \tau_{rz}=0
\end{aligned} \tag{A3}$$

For a vertical well, it simplifies to:

$$\begin{aligned}
\sigma_r &= p_{\mathrm{mud}}\\
\sigma_\theta &= \sigma_H+\sigma_h-2(\sigma_H-\sigma_h)\cos 2\theta-p_{\mathrm{mud}}\\
\sigma_z &= \sigma_v-2\nu(\sigma_H-\sigma_h)\cos 2\theta\\
\tau_{\theta z} &= \tau_{r\theta}=\tau_{rz}=0
\end{aligned} \tag{A4}$$

Therefore, the minimum and maximum tangential stresses at the wellbore wall in a vertical well can be obtained:

$$\begin{aligned}
\sigma_\theta^{\min} &= 3\sigma_h-\sigma_H-p_{\mathrm{mud}} \quad \theta=0^\circ\\
\sigma_\theta^{\max} &= 3\sigma_H-\sigma_h-p_{\mathrm{mud}} \quad \theta=90^\circ
\end{aligned} \tag{A5}$$

The principal effective stresses around the wellbore wall can be calculated from the stress components shown in Eq. (A3) by applying Biot's effective law [60]:

$$\sigma' = \sigma-\alpha p_p \tag{A6}$$

where $\sigma$ and $\sigma'$ are the total and effective stresses, respectively.

Notice that the radial stress at wellbore wall ($\sigma_r$) is always one of the three principal stresses. Therefore, in an inclined borehole we only need to calculate the principal stresses in ($\theta$, $z$) plane, as shown in Fig. 2(c), using the following equations:

$$\sigma'_{\theta\max} = \frac{1}{2}\left(\sigma_\theta+\sigma_z+\sqrt{(\sigma_\theta-\sigma_z)^2+4\tau_{\theta z}^2}\right)-\alpha p_p \tag{A7}$$

$$\sigma'_{\theta\min} = \frac{1}{2}\left(\sigma_\theta+\sigma_z-\sqrt{(\sigma_\theta-\sigma_z)^2+4\tau_{\theta z}^2}\right)-\alpha p_p \tag{A8}$$

$$\sigma'_r = p_{\mathrm{mud}}-\alpha p_p \tag{A9}$$

$$\tan 2\gamma = \frac{2\tau_{\theta z}}{\sigma_\theta-\sigma_z} \tag{A10}$$

where $\sigma'_{\theta\max}$, $\sigma'_{\theta\min}$ are the maximum and minimum effective principal stresses in ($\theta$, $z$) plane; $\sigma'_r$ is the effective principal radial stress in ($r$,$\theta$) plane; $\gamma$ is the angle between $\sigma_{\theta\max}$ and $\sigma_\theta$.

When stresses at the wellbore wall exceed the rock strength, wellbore starts to fail. The Mohr–Coulomb failure criterion (Eq. (9)) can be used to determine the wellbore shear failure. In shear failure condition, $\sigma'_r$ is the minimum stress, i.e., $\sigma'_3=\sigma'_r$; therefore, $\sigma'_1=\sigma'_{\theta\max}$. Substituting Eqs. (A7 and A9)) to Eq. (9) the mud pressure, or shear failure pressure $p_{\mathrm{mud}}$, to prevent shear failure around an inclined wellbore wall can be obtained from the following equation:

$$\frac{1}{2}\left(\sigma_\theta+\sigma_z+\sqrt{(\sigma_z-\sigma_\theta)^2+4\tau_{\theta z}^2}\right)-p_p=UCS+q\left(p_{\mathrm{mud}}-\alpha p_p\right) \qquad \text{(A11)}$$

From Eq. (A11), we can solve the shear failure pressure $p_{\mathrm{mud}}$, but notice that $\sigma_\theta$ in Eq. (A11) (can be obtained from Eq. (A3)) also includes $p_{\mathrm{mud}}$.

For the shear failure (slip failure) in the weak planes in an inclined borehole, by substituting Eqs. (A7 and A9) to Eq. (13) we obtain the following equation to calculate the minimum mud pressure (slip-failure pressure, $p_w^{\mathrm{incl}}$) for preventing wellbore sliding failure in the weak planes:

$$\frac{1}{2}\left(\sigma_\theta+\sigma_z+\sqrt{(\sigma_\theta-\sigma_z)^2+4\tau_{\theta z}^2}\right)-p_w^{\mathrm{incl}}=\frac{2\left[c_w+\mu_w\left(p_w^{\mathrm{incl}}-p_p\right)\right]}{(1-\mu_w\cot\beta)\sin 2\beta} \qquad \text{(A12)}$$

The weak plane slip-failure pressure $p_w^{\mathrm{incl}}$ can be solved from Eq. (A12). It should be noted that $\sigma_\theta$ can be obtained from Eq. (A3) with replacing $p_{\mathrm{mud}}$ to $p_w^{\mathrm{incl}}$.

## References


[1] Li S, George J, Purdy C. Pore pressure and wellbore stability prediction to increase drilling efficiency. J Petrol Technol 2012;64:98–101.
[2] Bradley WB. Failure of inclined boreholes. J Energy Res Technol 1979;101:232–9.
[3] Plumb RA, Hickman SA. Stress-induced borehole elongation: a comparison between the four-arm dipmeter and the borehole televiewer in the Auburn geothermal well. J Geophys Res 1985;90:5513–21.
[4] Zoback MD, Moos D, Mastin L. Well bore breakouts and in situ stress. J Geophys Res 1985;90(B7):5523–30.
[5] Woodland DC. Borehole instability in the Western Canadian overthrust belt. SPE Drilling Eng 1990;5:23–33.
[6] Roegiers JC. Stability and failure of circular openings. In: Rock at great depth, Maury & Fourmaintraux, editor, Balkema, Rotterdam; 1990. p.1115–1121.
[7] Detournay E, AHD. Cheng. Poroelastic response of a borehole in a non-hydrostatic stress field. Int J Rock Mech Min Sci Geomech Abstr 1988;25(3):171–82.
[8] Ewy RT. Wellbore stability prediction using a modified Lade criterion. paper SPE/ISRM 47251, 1998.
[9] Willson SM, Last NC, Zoback MD, Moos D. Drilling in South America: a wellbore stability approach for complex geologic conditions. Paper SPE 53940 presented at Latin America and Caribbean petroleum engineering conference held in Caracas, Venezuela; 1999.
[10] van Oort E. On the physical and chemical stability of shales. J Petrol Sci Eng 2003;38:213–35.
[11] Zhang J, Bai M, Roegiers JC. Dual-porosity poroelastic analyses of wellbore stability. Int J Rock Mech Min Sci 2003;40:473–83.
[12] Zhang J, Roegiers JC. Double porosity finite element method for borehole modeling. Rock Mech Rock Eng 2005;38(3):217–42.
[13] Zhang J, Bai M, Roegiers JC. On drilling directions for optimizing horizontal well stability using a dual-porosity poroelastic approach. J Petrol Sci Eng 2006;53:61–76.
[14] Haimson B, Lee H. Borehole breakouts and compaction bands in two high-porosity sandstones. Int J Rock Mech Min Sci 2004;4:287–301.
[15] Zhang J, Roegiers JC. Double porosity finite element method for borehole modeling. Rock Mech Rock Eng 2005;38:217–42.
[16] Zhang J, Standifird W, Lenamond C. Casing ultradeep, ultralong salt sections in deep water: a case study for failure diagnosis and risk mitigation in record-depth well. Paper SPE 114273, presented at SPE annual technical conference & exhibition, Denver; 2008.
[17] Aadnoy B, Chenevert ME. Stability of highly inclined boreholes. SPE Drill Eng 1987:364–74 December.
[18] Zhang J, Lang J, Standifird W. Stress, porosity, and failure dependent compressional and shear velocity ratio and its application to wellbore stability. J Petrol Sci Eng 2009;69:193–202.
[19] Dresen G, Stanchits S, Rybacki E. Borehole breakout evolution through acoustic emission location analysis. Int J Rock Mech Min Sci 2010;47:426–35.
[20] Gelet R, Loret B, Khalili N. Borehole stability analysis in a thermoporoelastic dual-porosity medium. Int J Rock Mech Min Sci 2012;50:65–76.
[21] Lang J, Li S, Zhang J Wellbore stability modeling and real-time surveillance for deepwater drilling to weak bedding planes and depleted reservoirs. Paper SPE/IADC 139708, presented at the SPE/IADC drilling conference and exhibition held in Amsterdam, The Netherlands; 2011.
[22] Ong SH, Roegiers JC. Influence of anisotropies in borehole stability. Int J Rock Mech Min Sci 1993;30(7):1069–75.
[23] Okland D, Cook JM. Bedding-related borehole instability in high-angle wells. Paper SPE/ISRM 47285; 1998.
[24] Willson SM, Edwards ST, Crook A, Bere A, Moos D, Peska P. Assuring stability in extended-reach wells—analyses, practice, and mitigations. Paper SPE/IADC 105405; 2007.
[25] Aadnoy B, Hareland G, Kustamsi A, de Freitas T, Hayes J. Borehole failure related to bedding plane. Paper ARMA 09-106, presented at the 43rd US rock mechanics Asheville, NC; 2009.
[26] Santarelli FJ, Dahen D, Baroudi H, Sliman KB. Mechanisms of borehole instability in heavily fractured rock media. Int J Rock Mech Min Sci 1992;29:457–67.
[27] Popp T, Salzer K, Minkley W. Influence of bedding planes to EDZ-evolution and the coupled HM properties of Opalinus Clay. Phys Chem, Earth 2008;33:S374–87.
[28] Gaede O, Karpfinger F, Jocker J, Prioul R. Comparison between analytical and 3D finite element solutions for borehole stresses in anisotropic elastic rock. Int J Rock Mech Min Sci 2012;51:53–63.
[29] Peng S, Zhang J. Engineering geology for underground rocks. Berlin: Springer; 2007.
[30] Zoback MD. Reservoir geomechanics. Cambridge: Cambridge Univ. Press; 2007.
[31] Fjær E, Holt RM, Horsrud P, Raaen AM. Petroleum related rock mechanics. 2nd ed. Oxford: Elsevier; 2008.
[32] Zhang J. Pore pressure prediction from well logs: methods, modifications, and new approaches. Earth Sci Rev 2011;108:50–63.
[33] Haimson BC, Cornet FH. ISRM suggested methods for rock stress estimation—Part 3: Hydraulic fracturing (HF) and/or hydraulic testing of pre-existing fractures (HTPF). Int J Rock Mech Min Sci. 2003;40:1011–20.
[34] Zhang J, Roegiers JC. Discussion on Integrating borehole-breakout dimensions, strength criteria, and leak-off test results, to constrain the state of stress across the Chelungpu Fault, Taiwan. Tectonophysics 2010;492:295–8.
[35] Meng Z, Zhang J, Wang R. In-situ stress, pore pressure and stress-dependent permeability in the Southern Qinshui Basin. Int J Rock Mech Min Sci 2011;48(1):122–31.
[36] Li S, Purdy C. Maximum horizontal stress and wellbore stability while drilling: modeling and case study. Paper SPE139280, presented at the SPE Latin American & Caribbean petroleum engineering conference held in Lima, Peru; 1–3 December 2010.
[37] Lal M. Shale stability: drilling fluid interaction and shale strength. Paper SPE 54356; 1999.
[38] Horsrud P. Estimating mechanical properties of shale from empirical correlations. SPE Drill Compl 2001;16:68–73.
[39] Kranz RL. The effects of confining pressure and stress difference on static fatigue of granite. J Geophys Res 1980;85(B4):1854–66.
[40] Kurita K, Swanson PL, Getting IC, Spetzler H. Surface deformation of westerly granite during creep. Geophys Res Lett 1983;10(1):75–8.
[41] Masuda K. Effects of water on rock strength in a brittle regime. J Struct Geol 2001;23(11):1653–7.
[42] Greenwood J, Bowler P, Sarmiento JF, Wilson S, Edwards S Evaluation and application of real-time image and caliper data as part of a wellbore stability monitoring provision. Paper IADC/SPE 99111; 2006.
[43] Schmidtke RH, Lajtai EZ. The long-term strength of Lac du Bennet granite. Int J Rock Mech Min Sci Geomech Abstr 1985;22:461–5.
[44] Al-Ajmi AM, Zimmerman RW. Relation between the Mogi and the Coulomb failure criteria. Int J Rock Mech Min Sci 2005;42:431–9.
[45] Zhang J, Roegiers JC. Borehole stability in naturally deformable fractured reservoirs—a fully coupled approach. Paper SPE 77355, presented at SPE annual technical conference and exhibition held in San Antonio, TX; 2002.
[46] Addis MA, Barton NR, Bandis SC, Henry JP. Laboratory studies on the stability of vertical and deviated boreholes. Paper SPE 20406; 1990.
[47] Barton N. Rock quality, seismic velocity, attenuation and anisotropy. London: Taylor & Francis; 2007.
[48] Bandis S. Personal communication. 2011.
[49] Thiercelin MJ, Plumb RA. Core-based prediction of lithologic stress contrasts in east Texas formations. SPE Form Eval 1994;9(4):251–8.
[50] Donath FA. Strength variation and deformational behavior in anisotropic rock. In: Judd WR, editor. State of stress in the Earth's crust. New York: Elsevier; 1964. p. 281–97.
[51] Donath FA. Faulting across discontinuities in anisotropic rock. Stability of rock slopes. In: Cording, E J, editor. Proceedings of 13th symposium. Rock Mech., Urbana, Ill., Aug/Sept 1971. New York: Am Soc Civ Eng p. 753–772.
[52] McLamore R, Gray KE. The mechanical behavior of anisotropic sedimentary rocks. J Eng Indust 1967;89:62–73.
[53] Amadei B. Importance of anisotropy when estimating and measuring in situ stresses in rock. Int J Rock Mech Min Sci Geomech Abstr 1996;33(3):293–325.

[54] Niandou H, Shao JF, Henry JP, Fourmaintraux D. Laboratory investigation of the behaviour of Tournemire shale. Int J Rock Mech Min Sci 1997;34(1):3–16.
[55] Brady BHG, Brown ET. Rock mechanics for underground mining. Berlin: Springer; 2004.
[56] Mogi K. Experimental rock mechanics. London: Taylor & Francis; 2007.
[57] Naumann M, Hunsche U, Schulze O. Experimental investigations on anisotropy in dilatancy, failure and creep of Opalinus Clay. Phys Chem Earth 2007;32:889–95.
[58] Jaeger JC, Cook NGW, Zimmerman RW. Fundamentals of rock mechanics. 4th ed. Oxford: Wiley-Blackwell; 2007.
[59] Zhang J Dual-porosity approach to wellbore stability in naturally fractured reservoirs. PhD dissertation. University of Oklahoma; 2002.
[60] Biot M. General theory of three dimensional consolidation. J Appl Phys 1941;12:155–64.